

On Cosine-fourth and Vignetting Effects in Real Lenses*

Manoj Aggarwal Hong Hua Narendra Ahuja
University of Illinois at Urbana-Champaign
405 N. Mathews Ave, Urbana, IL 61801, USA
{manoj,honghua,ahuja}@vision.ai.uiuc.edu

Abstract

This paper has been prompted by observations of disparities between the observed fall-off in irradiance for off-axis points and that accounted for by the cosine-fourth and vignetting effects. A closer examination of the image formation process for real lenses revealed that even in the absence of vignetting a point light source does not uniformly illuminate the aperture, an effect known as pupil aberration. For example, we found the variation for a 16mm lens to be as large as 31% for a field angle of 10° . In this paper, we critically evaluate the roles of cosine-fourth and vignetting effects and demonstrate the significance of the pupil aberration on the fall-off in irradiance away from image center. The pupil aberration effect strongly depends on the aperture size and shape and this dependence has been demonstrated through two sets of experiments with three real lenses. The effect of pupil aberration is thus a third important cause of fall in irradiance away from the image center in addition to the familiar cosine-fourth and vignetting effects, that must be taken into account in applications that rely heavily on photometric variation such as shape from shading and mosaicing.

1. Introduction

This paper has been prompted by observations of disparities between the observed photometric mappings between the scene and its image, and those predicted by standard models of image formation. The two effects that are commonly used to describe this relationship are the cosine-fourth and vignetting effects. We recently investigated these effects in the context of mosaicing a sequence of images acquired by a rotating camera to generate a panoramic image. The processes involved selection of pixels from different images and their compilation into a single image. Since, the camera is rotating,

*The authors gratefully acknowledge the support of a grant from Advanced Telecommunication Research International, Japan.

a scene point may occur in different directions at different times, and therefore, may have different brightness values in different images due to nonuniform photometric sensitivity of the camera. This requires a brightness correction function for normalization. We computed this correction function based on the cosine-fourth effect and observed significant discrepancies between the computed correction function and the one determined experimentally, even when using small apertures in which case vignetting is absent. These observations led us to more closely examine the photometric mapping. In this paper, we critically evaluate the familiar cosine-fourth and vignetting effects in real lenses and also presents the effect of an additional unexplored but significant imaging phenomenon called *pupil aberration* on the relationship.

A commonly used model for image formation is the Gaussian thick-lens model. In this model, the image irradiance of off-axis points falls off as cosine-fourth of the angle α that the line joining a point with the lens center makes with the optical axis [3]. This fall-off in irradiance is popularly known as the *cosine-fourth* radiometric effect. In typical lens systems, the fall-off is observed to be steeper than predicted by the cosine-fourth effect. The additional loss of irradiance is typically attributed to *vignetting*, which is illustrated in Fig. 1 As seen in the figure, a parallel beam of rays from a far away axial point fully illuminates the aperture. However, the beam emanating from a far away, off axis point is obstructed by the lens elements and is unable to completely fill the physical aperture [4, 5]. The extent of vignetting strongly depends on the dimensions of the aperture. Consider the aperture for the lens in Fig. 1 as it is reduced from AA' to BB' . Then for all objects within an elevation of α , there is no vignetting, which is not the case when aperture is equal to AA' .

When vignetting occurs for a point object only a smaller portion of the entire aperture contributes light to the image of that object. In that sense, the effective aperture seen by the object point is smaller. Since, the amount of aperture that contributes light varies with angular position of the object point, vignetting

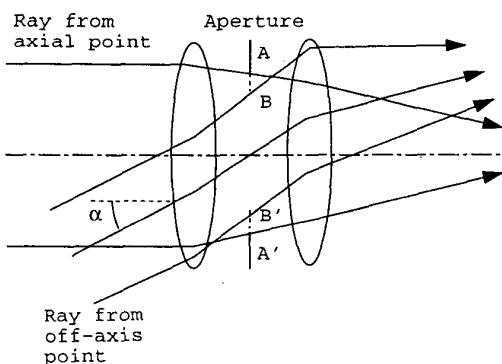


Figure 1. Vignetting

effectively causes a change in the shape and size of the aperture as seen from different angular positions. Vignetting is usually more dominant than the cosine-fourth for large apertures (smaller f-number) and absent for smaller apertures (larger f-number). This implies that for smaller aperture, the observed photometric mapping must closely match the behavior as predicted by the cosine-fourth effect. However, in the experiments that we have conducted on three real lenses, we have observed mappings that could not be explained using cosine-fourth and vignetting effects, alone. The experiments also provide evidence of the significance of a hitherto unexplored phenomenon called pupil aberrations in image formation, in addition to those of cosine-fourth and vignetting.

Pupil aberration is a phenomenon related to variation in the amount of light that is allowed to pass through the lens as a function of angular position, which is in addition to the foreshortening effect. In the Gaussian thick-lens model, the aperture is assumed to be uniformly illuminated by the object point. However, in real lenses, due to the nonlinear refraction through the lens elements, the distribution of light across the aperture plane is not uniform, and the degree of non-uniformity is a function of the angular position of the point object. Thus, the amount of light flux that is allowed to pass through the lens, i.e. the integral of light distribution across the aperture, varies with the angular position of the object [1, 4]. This phenomenon is called pupil aberration and as we will show can significantly influence the fall-off behavior.

In Sec. 2, we first describe the pupil aberration phenomenon and discuss its potential impact on the photometric mapping. In Sec. 3 we document the experiments and our observations that prove the inadequacy of the cosine-fourth and vignetting effects to correctly model the fall-off behavior, and present qualitative arguments as to how pupil aberration phenomenon may

explain the observed behavior. This paper primarily focuses on the qualitative roles of various photometric phenomena, which would be useful to better understand the image formation process and pave the way for future research to quantitatively model the three photometric effects.

2. Pupil Aberrations

Consider an off-axis point light source which illuminates a lens. The various rays that enter the lens reach the aperture after multiple refractions given by Snell's law [2]. We know from basic optics that this nonlinear refraction of the rays results in a significantly nonuniform light distribution across the aperture [4, 1].

We theoretically evaluated the light distribution across the aperture for a sample lens available in the optical design software CODE-V. We chose the double-Gauss 100mm lens configuration which was scaled down to a lens of focal length 16mm. The light distribution on a circular section of the aperture aligned with the optical axis due to three point sources at infinity and elevation angles 0° , 5° and 10° , respectively, are shown in Fig. 2.

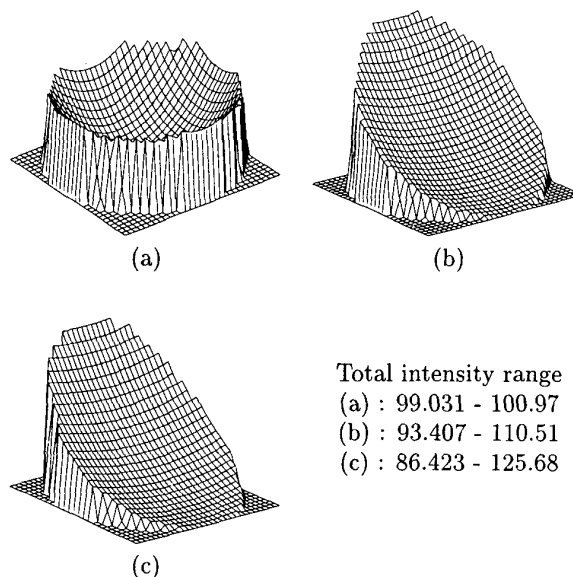


Figure 2. The light distribution across an aperture of diameter 3mm when the point light source located at infinity and an elevation angle of: (a) 0° , (b) 5° , and (c) 10° .

The light distribution plot for field angle 0° is circu-

larly symmetric, i.e. it is independent of the azimuth angle, while those for field angles 5° and 10° involve larger intensities at one end of the aperture and lower towards the other. The percentage decreases in the light distribution from one end to the other for 5° and 10° field angles are 15.47% and 31.23%, respectively.

The amount of light from a point source that is allowed through the lens is given by the integral of the light distribution across the aperture. To get a quick insight into the effect of the nonuniformity of light distribution, consider a planar approximation to the light distribution shown in Fig. 2(c) and the following two cases. First, assume that the centroid of the aperture is located on the optical axis where the aperture plane intersects it. Let the slope of the planar light distribution be s_x and s_y along the x and y axes. Then the integral of the planar light distribution over the aperture is given by the product of the aperture area and the value of the light distribution at the centroid. This holds irrespective of the actual shape of the aperture. Clearly, the integral is also independent of any rotations of the aperture about the centroid. Thus, if the centroid of the aperture is aligned with the optical axis, the impact of pupil aberration on the fall-off is unaffected by aperture rotation. Second, consider the situation when the centroid of the aperture does not coincide with the optical axis. In this case, the position of the centroid will change for different orientations of the lens, which implies that the value of the integral and hence the amount of light that is allowed to pass through will also change. This means that fall-off surface will not be circularly symmetric.

The non-uniform distribution of light in the aperture, therefore, has a two-fold impact on the fall-off behavior. First, for a given aperture as the elevation angle increases the integral of the light distribution over the aperture changes and so does the amount of light that is allowed through. Second, for a given elevation angle, the fall-off behavior may not be circularly symmetric. Due to the first effect, the maximum difference between the fall-off surfaces over the entire half-field of 10° for the sample double-Gauss lens was found to be 0.5%. However, the second factor turned out to be much more significant. For example, even a 0.1mm offset in the centroid of a 3mm diameter aperture for the sample double-Gauss lens lead to a variation of 1.2% for the same elevation but over the entire 2π range of azimuth angle.

The second case, that of the centroid being off-axis, is indeed the case for real lenses. In real lenses, iris is comprised of several mechanical leaves that move in and out to realize user desired changes in f-number. The coherence and accuracy of the movements of the leaves is not high enough to ensure symmetry in the

iris shape, and thus the centroid is not a fixed point. The result is a continuous perturbation in the location of the iris in the vicinity of a fixed point as the f-number is varied. This effect is particularly severe for smaller aperture sizes for two reasons. First, the deviation of the centroid becomes an increasingly large fraction of the iris size as the iris closes. Second, in many lenses (e.g., Navitar D01614, DO2516, Cosmicar 22525), very small f-numbers are realized by moving only some of the leaves (e.g., one), and this leads to even greater asymmetry in the iris shape.

The variability in the illuminated area of the aperture also adversely affects the modeling of vignetting. Vignetting results in only a part of the iris getting illuminated. The larger the elevation angle, the more skewed and smaller is the illuminated area. The intersection of the illuminated area and the aperture changes in a complex manner with the elevation and azimuth angles, causing further shifts in the centroid, and thus poorer predictability of irradiance.

Motivated by these preliminary observations and arguments, we conducted some experiments to verify and document the effects of pupil aberration on the fall-off behavior. These experiments are reported in the next section.

3. Experiments

The first experiment records the fall-off surface for various aperture settings and the second experiment deals with capturing the shape and size of the aperture under different aperture settings and from different elevation and azimuthal angles.

3.1. Experimental setup

The experimental setup used consisted of a uniform, lambertian, extended light source placed parallel to the lens-mount. The light source used was a light box KLV7000 (www.hakubausa.com). The fall-off surfaces under a fixed camera configuration were found to be slightly different for different positions of the light box, which indicated that the light source was not sufficiently uniform. To improve the uniformity, we added a few light diffusing elements (flushed opal and plexi glass sheets) as the front side of the light box. The modified light box was tested to give identical fall-off surfaces.

The camera used for the experiments was a Pulnix TM720, whose lens mount had been decoupled from the camera housing containing the sensor and the rest of the electronics. The camera housing was mounted on a six-stage positioner (three for translation and three for rotation). These modifications to the camera allowed us to perform tasks such as changing the focal settings,

aligning the image center to the optical center and placing the sensor normal to the optical axis.

There are two parameters that need to be controlled as a part of the experimental setup that could confound the relationship of the image irradiance to the variables under study, namely those contributing to pupil aberration and vignetting. These include sensor tilt (sensor not perpendicular to optical axis) and light source tilt. The effects of these parameters must be eliminated in our experiments. In the next section, we will briefly discuss the effects of these spurious parameters, and the steps we took to circumvent them.

3.2. Circumventing tilt effects

The effect of light source tilt has insignificant impact on the fall-off behavior because the depth variation caused by small tilts is quite small compared to the distance from the mount surface. We experimentally verified the above assertion by estimating the fall-off surfaces over a narrow range of tilts (within $\pm 10^\circ$). The resulting fall-off surfaces were found to be very close to each other. In contrast, sensor tilt has a significant impact on the fall-off surface, because of its close proximity to the lens. We observed that the sensor tilts necessary to ensure that the fall-off surfaces are symmetric, were different for different aperture settings. A yet another tilt was needed to uniformly focus the sensor on a planar chart placed parallel to the lens mount surface. These tilt angles had a range of about 1.5° .

Sensor tilt modulates the intensity distribution by reducing the irradiance of points farther away from the lens and increasing it for closer points. Since, we cannot eliminate the asymmetry due to sensor tilt, we propose to observe the variation in irradiance only along the middle row of the sensor and as a function of the rotation of the lens. This approach has the advantage that we are able to observe the fall-off behavior along different azimuth angles without subjecting them to different modulation functions due to sensor tilt. This enables inferences to be drawn about the shape of the fall-off behavior even in the presence of bias caused by the sensor tilt. For example, for a circularly symmetric lens configuration, the fall-off curves are possibly asymmetric but must be identical under different rotations of the lens.

3.3. Impact of pupil aberrations

Experiment IOA (Imaging the effective aperture): A grid of point light sources was generated by placing a thick black colored sheet with a uniform grid of pinholes on the front surface of the modified light box. The sensor was moved closer to the lens with respect to the conjugate position and images were cap-

tured for three different aperture settings $f = 1.6, 2, 4$. The images corresponding to the three lenses are shown in Fig. 5 (Navitar DO1614), Fig. 7 (Cosmicar 22525) and Fig. 9 (Tamron 23FM25). Each image consists of a number of blurred subimages which represent the point spread function (PSF) of the lens under different elevation and azimuth angles. The point spread function reflects the shape of effective aperture seen from a particular elevation and azimuth angle.

Observations: The primary observation for all three lenses is that the images of the effective aperture for the larger aperture sizes are circular in the middle and become oval towards the edges. Further, the centers of the PSF's are further apart on the periphery than towards the center. In contrast the grid of PSFs for aperture setting 4 (i.e smaller aperture sizes) are more regular and almost identical to each other. There are two conclusions one can draw from these observations. First, the vignetting effect is present for aperture settings 2 and 1.6 and absent for setting 4. Second, the position of the centroid of the effective aperture is a function of aperture setting, and the distance between the optical axis and the centroid can become quite large due to vignetting for off-axis points.

In another similar experiment we recorded the shape of the PSF under aperture setting 16 for the three lenses shown in Fig. 3. The aperture for Navitar DO1614 at $f = 16$ is no longer a regular pentagon as in Fig 5(c) and most likely has a different centroid than for the larger apertures. The aperture for Cosmicar 22525 at $f = 16$ is symmetric, but its shape is different from those it has for the larger aperture sizes shown in Fig. 7 which would also have different centroids. The aperture at $f = 16$ for Tamron 23FM25 lens is a regular hexagon. Even though the larger apertures have different shapes (Fig. 9), they have even symmetry which ensures that their centroids are the same.

This experiment illustrates the dependence of vignetting on aperture settings, the large extent of disparity that exists between the centroid of the aperture and the optical axis, and the dependence of the disparity on the aperture setting and the direction of view. The next set of experiments concerns the impact of the displacement of the centroid on the fall-off behavior.

Experiment FOC (Fall-off curves): We placed the modified light box at a distance of 205mm from the front surface of the lens mount. The sensor position and tilt were chosen such that the light surface is conjugate. The conjugacy was ensured by placing a printed sheet of paper on the light source surface and then used the 6-stage positioner to orient the sensor such that the image of printed sheet is in focus. The optical or principal center was manually aligned to the image center, as a

precise alignment was not necessary for this experiment (misalignment would only shift a fall-curve).

Images were acquired for six different settings of the aperture and the fall-off curves are plotted in Fig. 4 (Navitar DO1614), Fig. 6 (Cosmicar C22525) and Fig. 8 (Tamron 23FM25). Each figure consists of three subplots (a), (b) and (c). Subplot (a) plots the fall-off curves for different aperture settings $f = 16.0, 8.0, 4.0, 2.8, 2.0, 1.6$. Plots (b) and (c), which we refer to as the rotation plots show the fall-off curves under 6 different rotations of the lens, for the smallest f-number and the largest f-number on the lens, respectively. Each curve in each plot has been individually normalized by scaling it by the inverse of the maximum value, and then vertically shifted with respect to the other curves to avoid their mutual overlaying. The vertical location of the plots is therefore unimportant.

Observations:

- For each of the three lenses the fall-off curves have similar ranges of irradiance values for the f-numbers between 16 and 2.8. For f-numbers 2.8 and lower, the range of irradiance values increases rapidly. Incidentally, the fall-off curves do not coincide with the cosine-fourth curves for any of the aperture settings.
- The fall-off curves for different lens rotations for the lowest f-number (Figs. 4(b), 6(b), 8(b)) are almost identical, though unsymmetric.
- The fall-off curves for the highest f-number for the Navitar (Fig. 4(c)) and Cosmicar lens (Fig. 6(c)) vary as the lens is rotated while they remain largely unchanged for the Tamron lens (Fig. 8(c)).

The first observation shows that vignetting is absent for aperture settings larger than 4. The second observation suggests that lens decentrations have negligible impact on the fall-off behavior.

Based on Experiment IOA and the first two observations in Experiment FOC, we conclude that vignetting is absent for aperture settings higher than 4.0, and the effects of lens decentrations and small tilts in the sensor and the planar light source used for the experiment are negligible. In view of these conclusions, the third observation implies that the asymmetry observed for Cosmicar and Navitar lenses must be due to the shape and setting of the aperture, as that is the only factor different from the experiment where the aperture setting was the lowest.

It is clear from Figs. 4(c) and 6(c) that the effect of pupil aberration on the fall-off behavior is quite significant. For example, the upper-most and lower-most fall-off curves in Figs. 4(c) exhibit very different behaviors, and show a significant dependence on the azimuth

angle. The difference between the behavior of Navitar, Cosmicar and the Tamron lens can be attributed to differences in the locations of the centroids with respect to the optical axis, which is supported by the observations in the previous experiment on the shapes of the effective aperture for different aperture settings.

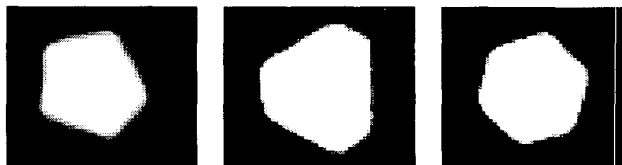


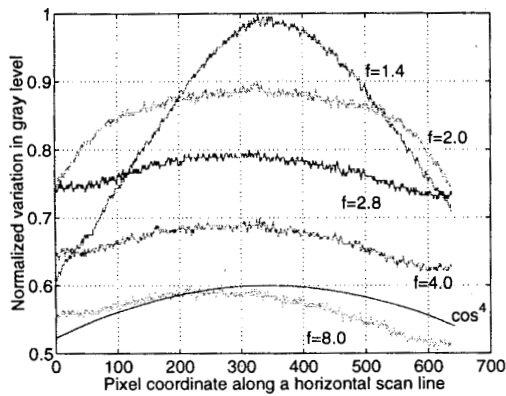
Figure 3. Images of the aperture for f-number 16. (a) Navitar DO1614: the sides are not of equal length; (b) Cosmicar 22525: though symmetric, the shape is not similar to that for lower aperture settings as in Fig. 7(c) and can have a different centroid, and (c) Tamron 23FM25: appears to be a regular hexagon, and should have the same centroid as that for the lower aperture setting in Fig. 9(c)

4. Conclusions

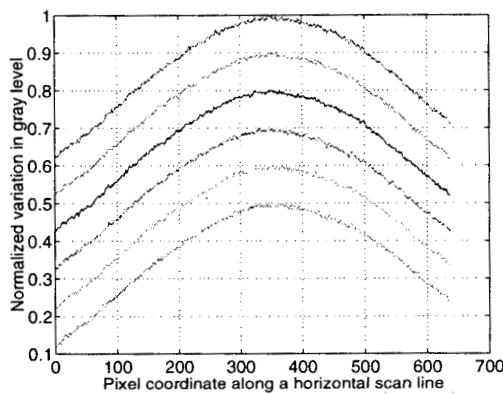
This paper critically evaluates the roles of cosine-fourth and vignetting effects, and describes the effect of an unexplored but significant radiometric phenomenon called pupil aberration on the relationship between the scene radiance and image irradiance. A consequence of pupil aberration is that the distribution of light on the aperture due a point source is nonuniform, and the distribution varies with the 3-D position of the point source. This nonuniformity results in a strong dependence of the relationship on the shape and f-number of the aperture. Experiments with three real lenses show that the phenomenon is quite significant in many common imaging scenarios.

References

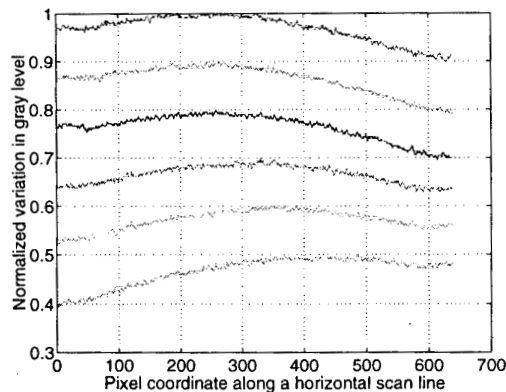
- [1] M. Born and E. Wolf. *Principles of optics: electromagnetic theory of propagation, interference and diffraction of light*. Cambridge University Press, 7th edition, 1999.
- [2] E. Hecht and A. Zajac. *Optics*. Addison Wesley, 1974.
- [3] B. K. P. Horn. *Robot Vision*. The MIT Press, Cambridge, Mass., 1986.
- [4] B. R. Johnson. Lenses. In *Handbook of Optics: Device Measurement and Properties*, volume II. McGraw Hill, 2nd edition, 1995.
- [5] R. Kingslake. *Optical System Design*. Academic Press, 1983.



(a)

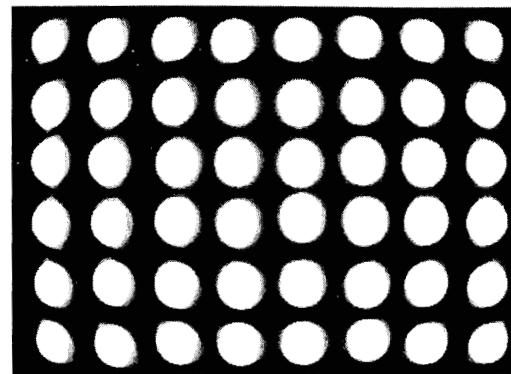


(b)

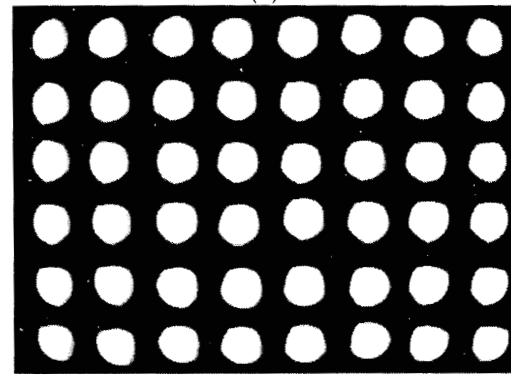


(c)

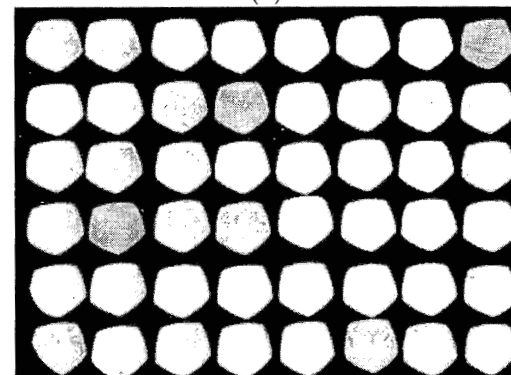
Figure 4. Fall off curves for Navitar 16mm lens (DO1614) (a) Comparison between the fall-off under different aperture settings; (b) Variation in the fall-off behavior for a fixed aperture setting of $f = 1.6$ under different rotations of the lens; (c) same as (b) except $f = 16$



(a)

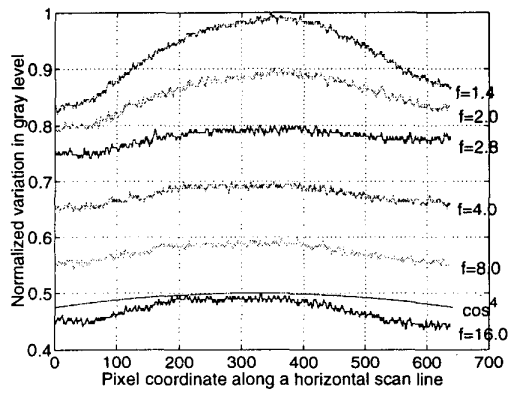


(b)

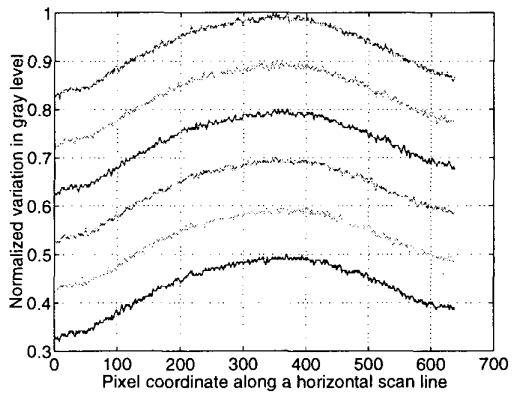


(c)

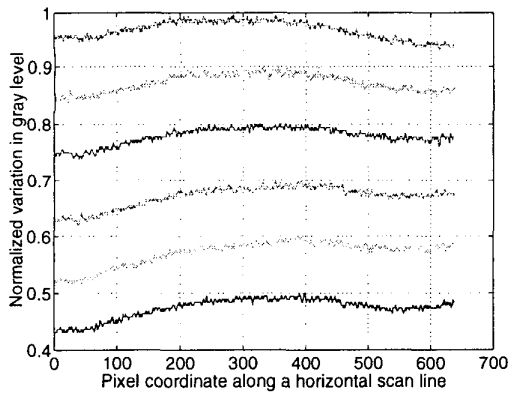
Figure 5. Blurred images of a frontal grid of point light sources acquired by Navitar (DO1614) lens; each bright patch can be considered as the point spread function corresponding to different x-y (spatial) positions of the the point source. These patches reflect the shape of the effective aperture as seen from different off-axis positions. (a) Aperture setting $f = 1.6$, (b) $f = 2$, (c) $f = 4$.



(a)

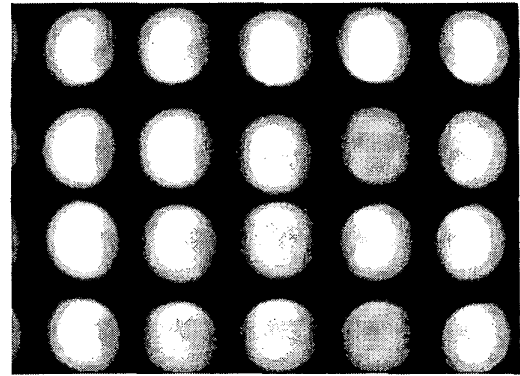


(b)

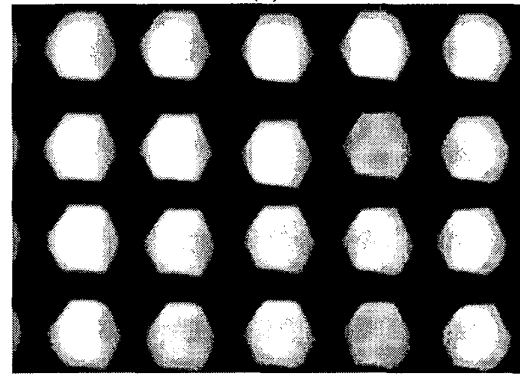


(c)

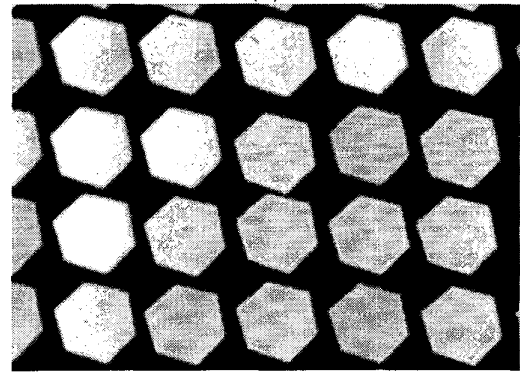
Figure 6. Fall off curves for Cosmicar 25mm lens (C22525) (a) Comparison between the fall-off under different aperture settings; (b) Variation in the fall-off behavior for a fixed aperture setting of $f = 1.4$ under different rotations of the lens; (c) same as (b) except $f = 16$



(a)

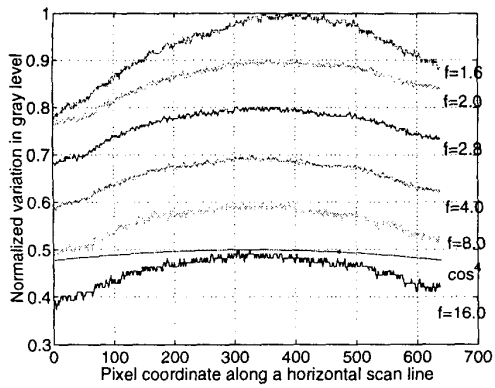


(b)

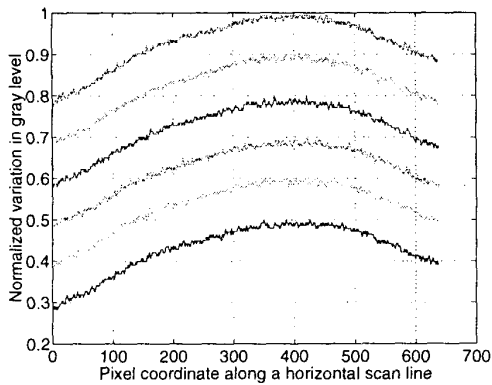


(c)

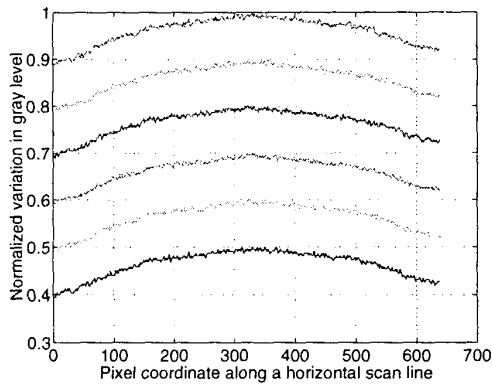
Figure 7. Blurred images of a frontal grid of point light sources acquired by Cosmicar (C22525) lens; each bright patch can be considered as the point spread function corresponding to different x-y (spatial) positions of the the point source. These patches reflect the shape of the effective aperture as seen from different off-axis positions. (a) Aperture setting $f = 1.6$, (b) $f = 2$, (c) $f = 4$.



(a)

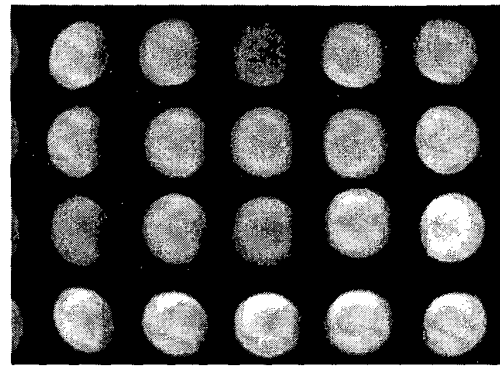


(b)

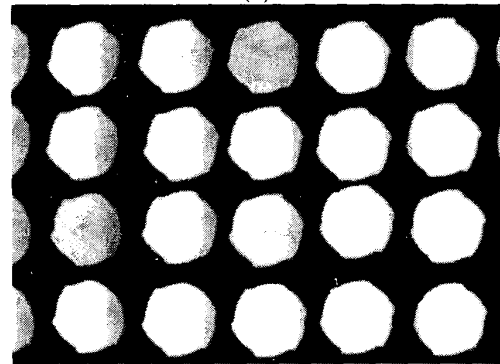


(c)

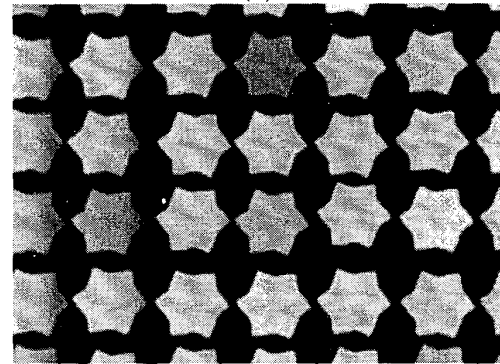
Figure 8. Fall off curves for Tamron 25mm lens (23FM25) (a) Comparison between the fall-off under different aperture settings; (b) Variation in the fall-off behavior for a fixed aperture setting of $f = 1.6$ under different rotations of the lens; (c) same as (b) except $f = 16$



(a)



(b)



(c)

Figure 9. Blurred images of a frontal grid of point light sources acquired by Tamron (23FM25) lens; each bright patch can be considered as the point spread function corresponding to different x-y (spatial) positions of the the point source. These patches reflect the shape of the effective aperture as seen from different off-axis positions. (a) Aperture setting $f = 1.6$, (b) $f = 2$, (c) $f = 4$.